Inorganic Chemistry

Article

pubs.acs.org/IC

First-Principles Study of Antisite Defect Configurations in $ZnGa_2O_4$:Cr Persistent Phosphors

Arthur De Vos,[†] Kurt Lejaeghere,[†] Danny E. P. Vanpoucke,[†,‡] Jonas J. Joos,[¶,§] Philippe F. Smet,*[,¶,§] and Karen Hemelsoet*[,†]

[†]Center for Molecular Modeling (CMM), Ghent University, Technologiepark 903, 9052 Zwijnaarde, Belgium

[‡]Center for Ordered Materials, Organometallics and Catalysis (COMOC), Department of Inorganic and Physical Chemistry, Ghent University, Krijgslaan 281 (S3), 9000 Ghent, Belgium

[¶]LumiLab, Department of Solid State Sciences, Ghent University, Krijgslaan 281 (S1), 9000 Ghent, Belgium

[§]Center for Nano- and Biophotonics, Ghent University, Sint-Pietersnieuwstraat 41, 9000 Ghent, Belgium

Supporting Information

ABSTRACT: Zinc gallate doped with chromium is a recently developed near-infrared emitting persistent phosphor, which is now extensively studied for in vivo bioimaging and security applications. The precise mechanism of this persistent luminescence relies on defects, in particular, on antisite defects and antisite pairs. A theoretical model combining the solid host, the dopant, and/or antisite defects is constructed to elucidate the mutual interactions in these complex materials. Energies of formation as well as dopant, and defect energies are calculated through density-functional theory simulations of large periodic supercells. The calculations support the chromium substitution on the slightly distorted octahedrally coordinated gallium site, and additional energy levels are introduced in the band gap of the host. Antisite pairs are found to be energetically favored over isolated antisites due to significant charge compensation as shown by calculated Hirshfeld-I charges. Significant structural distortions are found around all antisite defects. The local Cr surrounding is mainly distorted due to a Zn_{Ga} antisite. The stability analysis reveals that the distance between both antisites dominates the overall stability picture of the material containing the Cr dopant and an antisite pair. The findings are further rationalized using calculated densities of states and Hirshfeld-I charges.

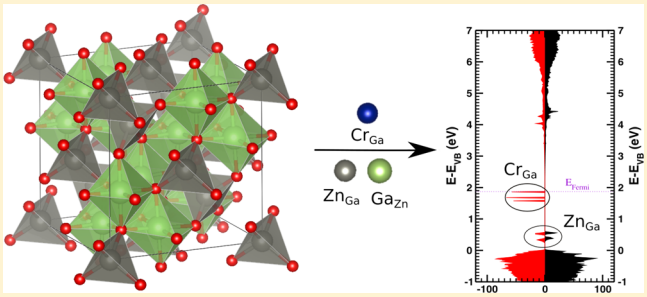

1. INTRODUCTION

Persistent luminescence is a specific type of photoluminescence in which the emission—usually in the visible or near-infrared range—can last for hours or even days after the irradiation source has been switched off.[1−4] The irradiation used may be visible or UV light, X-ray, or γ radiation. The long decay time of persistent luminescence is due to the storage of the excitation energy by traps. The traps originate from lattice defects, which are either intrinsically present or intentionally introduced. Subsequent detrapping and recombination yields the delayed luminescence.[2,3] Persistent phosphors are traditionally used in emergency signage and traffic signs, displays, toys, and gadgets. After the report on long and intense green persistent luminescence in $SrAl_2O_4$:Eu,Dy by Matsuzawa et al.,[5] the main focus was initially on divalent europium as emitting center, yielding emission in the blue-to-yellow, and occasionally in the orange-to-red part of the visible spectrum.[1] For these Eu^{2+}-based compounds, the trapping is presumably related to a photoionization of the europium center,[6] while the debate on the nature of the trapping center is still not settled. There is, however, an ongoing search for materials with outstanding luminescent properties that can be used for new applications. For example, the past five years have witnessed breakthroughs in applying persistent phosphors emitting in the near-infrared range for in vivo imaging. For this application, the emission spectrum of the phosphor should match with the transparency window of tissue. The lack of (infra)red-emitting Eu^{2+}-based persistent phosphors initiated investigations into other dopant ions, such as Mn^{2+} and Cr^{3+}, with many phosphors showing excellent storage capacity.[7−10] Chromium-doped zinc gallate (hereafter referred to as ZGO:Cr) is one of the most prominent materials in this emerging domain.[11−18] The luminescent Cr center can not only be excited under UV radiation but also by using orange-red light, which has the advantage that it is situated in the transparency window of living tissues, making in vivo excitation possible.

From a crystallographic point of view, ZGO belongs to the spinel structures AB_2O_4. For these compounds, A is typically a divalent ion (Zn, Mg, Ca, Sr), while B is trivalent (Al, Ga, Cr). In a normal spinel, the A ions are tetrahedrally coordinated with oxygen atoms, while the B ions occupy octahedral sites as

Received: December 3, 2015
Published: February 11, 2016

DOI: 10.1021/acs.inorgchem.5b02805
Inorg. Chem. 2016, 55, 2402−2412

shown in Figure 1. However, this site occupation can change depending on the composition, resulting in a mixed or even

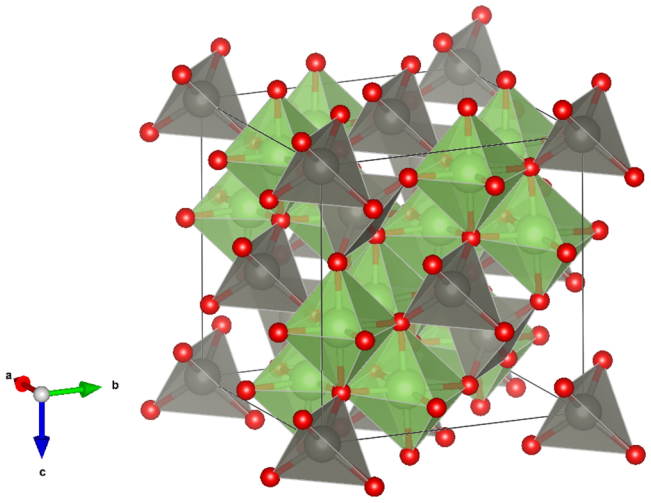

Figure 1. Spinel structure of ZGO displaying tetrahedrally coordinated Zn atoms (in gray) and octahedrally coordinated Ga atoms (in green). Oxygen atoms are shown in red.

inverse spinel. Occupational disorder results from the presence of antisite pairs, meaning that two atoms of the host exchange positions, and is often naturally present in these compounds.[19] When an antisite pair forms, the two sites bear a net charge, and a local electric field is created in the material. In the case of ZGO, the antisites correspond with a Zn^{2+} at a Ga site and a Ga^{3+} at a Zn site (denoted as Zn'_{Ga} and $Ga^{\bullet}_{Zn}$ in Kröger–Vink notation, respectively) forming the antisite pair. The concentration of naturally present antisite pairs is reported to be ~3%.[19] Careful electron paramagnetic resonance (EPR) spectroscopy and photoluminescence measurements revealed that these antisite pairs play a crucial role in the persistent luminescence mechanism in ZGO:Cr. In particular, Gourier et al. showed that excitation of specific Cr^{3+} ions with an antisite as first cationic neighbor leads to the crucial N2 lines observed in the emission spectra.[14] The trapping mechanism in this particular phosphor is different from the common case of Eu^{2+}-doped persistent phosphors, as no ionization of the Cr^{3+} dopants is expected. Instead, Gourier et al. suggested that two neighboring antisite defects, forming an antisite pair, create a local electric field at the Cr^{3+} dopant, which triggers charge separation upon excitation of the Cr^{3+} dopant.[14] A key element in this model is the suspected close proximity of both antisite defects.

To gain insight in the stability of the Cr^{3+} emission center and its interaction with antisites in the persistent ZGO phosphor, ab initio atomic-scale simulations can be used. The introduction of a dopant or defect induces changes in the structural and electronic properties that can be quantitatively determined much easier by simulations than experiments. In general, the inclusion of dopants introduces new energy levels in the band structure of the host. Knowledge of their exact positioning is crucial, as several models for persistent luminescence involve interactions between the conduction band (CB) levels of the host and the excited states of the dopant. The trap depth of the involved defects, being on the order of 0.5 to 1 eV, should also be obtained to generate a correct view of all energy levels involved.[2,3,20] One thereby must keep in mind that variations in trap depth on the order of 0.2 eV have a strong impact on the detrapping kinetics of persistent phosphors. In a recent review on the class of lanthanide materials by Joos et al., it was reported that standard deviations of 0.3–0.5 eV are still obtained for the relevant energy differences when empirical models are employed, corroborating the need for accurate first-principles results.[21] Multireference methods have been employed on embedded cluster models, providing insight in the electronic transitions of the dopant ions and in the corresponding excited-state dynamics.[22−29]

Given the complexity of persistent phosphors, their ab initio simulation is usually performed with the aid of density functional theory (DFT), which uses the electron density as its basic property and is mainly of interest due to its high accuracy at feasible computational cost. The choice of an approximate exchange-correlation functional determines the final accuracy that can be obtained. Structural properties are reported to be in fairly good agreement with experimental observations, even for relatively simple DFT functionals.[30] Moreover, Du comprehensively reviewed that DFT methods can produce correct trends in stability and emission energy of activators in optical materials.[31] For example, the influence of Mn^{4+} insertion on the local structures of a series of oxides and fluorides was rationalized based on DFT computations analyzing the activator-ligand hybridization strength.[32,33] Recent years have witnessed a noticeable evolution in first-principles calculations for point defects in solids, as recently reviewed by Freysoldt et al.[34] Dixit and co-workers investigated the formation energies of defects—in particular cation/anion vacancies and defects in which one type of cation is replaced by the other, an antisite—in the $ZnAl_2O_4$ spinel, which is very similar to the ZGO material considered here.[35] The relative stability of different charge states of the defects was evaluated. This information allows finding the thermodynamic transition level between two different charge states, defined as the Fermi level position for which the formation energies of the charge states are equal.[34] It was concluded that the Al_{Zn} antisite has the lowest formation energy and can act as a shallow donor.[35] Also in the case of Cr impurities in different host materials, the influence of the charge state has been assessed via theoretical simulations.[36−38] Substitutional defects in doped phosphors have also been theoretically investigated by Seijo and co-workers. DFT-based simulations on doped $Y_3Al_5O_{12}$ elucidated the interactions between defects with or without a dopant in their vicinity.[39−41] Obtaining accurate band gaps of solids has proven to be a challenging problem. The use of local (local density approximation) or semilocal (generalized gradient approximation) DFT functionals leads to theoretical band gaps that are too small when compared with experiment due to the self-interaction error.[42−45] Several advances, including the DFT+U method[46] and other electronic-structure methods such as hybrid DFT functionals[47] and GW,[48] are available to overcome this problem. These techniques, however, require careful fitting of the parameter U or come at a large additional computational cost. Dixit et al., for example, calculated the band gap of three ZnX_2O_4 spinels (with X = Al, Ga, and In).[49] They demonstrated that the experimental band gap of $ZnGa_2O_4$ can satisfactorily be predicted using GW and the modified Becke–Johnson (MBJ) potential approximation, giving values of 4.57 and 4.71 eV, respectively, in good agreement with the experimental value of 4.40–5.00 eV.[49]

DOI: 10.1021/acs.inorgchem.5b02805
Inorg. Chem. 2016, 55, 2402−2412

The aim of the present work is to gain a deeper understanding of the interplay between the chromium dopant and possible antisites and antisite pairs in ZGO via first-principles simulations. We hereby focus on qualitative trends, comparing different locations of the antisites and providing an in-depth analysis of the structural and energetic properties of systems including the dopant and/or antisites. Moreover, the influence of defects on the energy levels of the chromium center is discussed. The theoretical data also provide detailed insight in the local chromium environment and its distortion upon introduction of antisites.

This paper is structured as follows. In Section 2, the computational details of the employed models and the ab initio simulations are presented. The structural and electronic properties of the ZGO material, including Cr dopant and/or antisites, are discussed in Section 3, starting with the analysis of single antisites in the host (Section 3.1), after which the preferred substitution site of Cr in the defect-free ZGO host (Section 3.2) is discussed. From that point onward only the most stable Cr dopant site is considered, and its interaction with antisites is analyzed (single antisites and antisite pairs in Sections 3.3 and 3.4, respectively).

2. COMPUTATIONAL DETAILS

To determine defect properties in ZGO, a 112-atom supercell (SC) was used, constructed as 2 × 2 × 2 times the primitive unit cell. In this SC all atoms of the same atomic species (i.e., all 16 Zn, 32 Ga, or 64 O atoms) are symmetrically equivalent. The equilibrium volume of this SC (1213.754 Å^3) was extracted from a Birch–Murnaghan fit of the energy of the 56-atom conventional unit cell (see Figure 1).

All calculations were performed using the VASP package,[50,51] employing the PBE functional[52] and a projector-augmented wave[53,54] basis set with a kinetic energy cutoff of 800 eV. A 3 × 3 × 3 k-point grid was used to sample the Brillouin zone. These settings allowed energy convergence up to 1 × 10^{-4} eV. All structures were moreover relaxed using a conjugate gradient method with the energy convergence criterion set to 1 × 10^{-7} eV. As a result, the maximum force on an atom at the end of a relaxation was <1 meV/Å. Optimized values of relevant structural properties of the ZGO host are found to be in good agreement with experimental data (see Section S1 of the Supporting Information).

The chromium substitution was imposed either at a Ga (Cr_{Ga}) or a Zn (Cr_{Zn}) site, resulting, respectively, in $Zn_{(1-x)}$ Ga_2O_4:Cr_x and in $ZnGa_{(2-x)}O_4$:Cr_x, with x = 1/16 in the SC, denoted as ZGO:Cr_{Zn} and ZGO:Cr_{Ga}. This doping percentage is somewhat higher than the experimental one, but simulating a lower percentage is computationally not recommended given the large number of atoms already taken into account. Furthermore, the occurrence of Cr clustering at higher concentrations, which can experimentally be observed, is not allowed by construction, compensating for the too-high chromium concentration.

The employed 2 × 2 × 2 SC allows the construction of a large number of defect configurations combining the dopant and antisite pair. A total of 30 configurations were examined. All dopant and defect energies were calculated after optimizing the ionic positions inside the periodic cell. The resulting dopant and defect formation energies were also compared with those obtained in the 56-atom conventional cell to assess the influence of the cell size (see Section S2 of the Supporting Information).

The detailed configuration of an antisite pair depends on the location of its constituting antisites, the Ga_{Zn} and Zn_{Ga}, with respect to chromium, and their mutual distances to each other, denoted as ($d_1d_2d_3$). The different gallium and zinc coordination shells of ZGO:Cr_{Ga} are represented in Figure 2a, and the relevant distances are indicated in Figure 2b. In case of an antisite pair in the undoped ZGO host, the distance d_3 between the substitutions was varied (see Figure 2b), resulting in three distinct configurations. A selection of these configurations were found in different ZGO:Cr samples by their signature in EPR spectra by Gourier et. al and denoted as Cr_i (i = α, β, γ, δ, ϵ). The microscopic models underlying these EPR signals were denoted as X–Cr–Y for which X represents the *most perturbing*, that is, closest to the Cr_{Ga} center, antisite defect.[14] Table 1 summarizes the correspondence between the different notations and the more general notation used in this work.

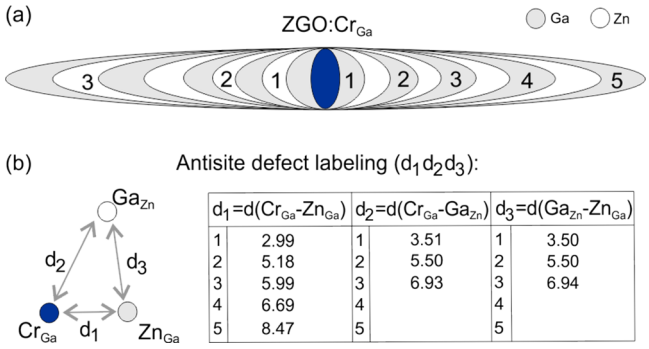

Figure 2. (a) Schematic representation of the Ga (in gray) and Zn (in white) coordination shells in ZGO:Cr_{Ga}, where the chromium dopant at the Ga position is shown in blue. (b) Relevant distances d_1, d_2, and d_3, used to characterize the ($d_1d_2d_3$) configurations of a chromium dopant and an antisite pair. The values before optimization are also reported (in Å).

Table 1. Nonequivalent Defect Configurations[a] Found from Electron Paramagnetic Resonance Spectroscopy and How These Are Specified by the General Notation Used in This Work

EPR signature	model by Gourier et al.	($d_1d_2d_3$)	
Cr_α	Cr_{Ga}		
Cr_β	Ga_{Zn}–Cr_{Ga}–Zn_{Ga}	(d_1 2 d_3)	$d_1 \geq 2$ and variable, d_3 unspecified
Cr_γ	Zn_{Ga}–Cr_{Ga}–Ga_{Zn}	(123)	
Cr_δ	Zn_{Ga}–Cr_{Ga}–Ga_{Zn}	(111)	
Cr_ϵ	Zn_{Ga}–Cr_{Ga}–Ga_{Zn}	(112)	

[a]There remains some uncertainty for the assignation of the Cr_δ and Cr_ϵ EPR signatures to structural models (111) and (112).[14]

Atomic charges of the systems were calculated using the iterative Hirshfeld-I approach as implemented in the HIVE code (version 3.x).[55−57] The implementation makes use of the grid-stored (pseudo) electron densities, which are standardly obtained from VASP. The atom-centered spherical integrations were done using Lebedev–Laikov grids of 1202 grid points per shell and a logarithmic radial grid.[58,59] The iterative scheme was considered converged when the largest difference in charge of a system atom was less than 1.0 × 10^{-5} electron in two consecutive iterations. All charges in this paper are given in units of e equal to 1.602 × 10^{-19} C.

3. RESULTS AND DISCUSSION

Defects are introduced in both the undoped ZGO host and the Cr-doped one. The Cr dopant is responsible for the luminescent properties of the material, but it is significantly influenced by the defects around it. The properties and stability of the defects, and more particularly of single antisites and antisite pairs, are therefore essential to explain the mechanism of persistent luminescence in the ZGO phosphor.

3.1. Single Antisites and Antisite Pairs in the Undoped ZGO Host. First the structural, energetic, and electronic effects of introducing antisites in the undoped ZGO

DOI: 10.1021/acs.inorgchem.5b02805
Inorg. Chem. 2016, 55, 2402−2412

host are studied. Initially, isolated antisites, that is, Zn_{Ga} or Ga_{Zn}, are considered, and next, the combination of two antisites into an antisite pair is discussed (denoted as $(00d_3)$).

3.1.1. Structural Properties. In the ZGO host, all atoms of a single atomic species (Zn, Ga, O) are equivalent, so replacement of one cation by another, introducing an antisite, leads to only two distinct materials. This inclusion of antisites in the undoped ZGO results in significant local structural changes. The distances to the nearest oxygen neighbors change: for Ga_{Zn} the bond length decreases by 4.5% (from 2.00 to 1.91 Å), and for Zn_{Ga} there is an increase of 3.0% (from 2.02 to 2.08 Å). In case of an antisite pair, the observed changes are very similar to those when only one antisite is introduced. The bond length decrease for Ga_{Zn} is again 3.0%, but for Zn_{Ga} the bond length now increases by 5.0% (from 2.02 to 2.12 Å). These changes are independent of the distance d_3. In all cases the change of bond length is equal for all four or six nearest oxygen neighbors.

3.1.2. Stability Analysis. The stability of the single antisites, Zn_{Ga} and Ga_{Zn}, can be estimated using either their formation or defect energy, as listed in Table 2. Both energies depend on the

Table 2. Formation Energy[a] ΔE_{form} for the Host, ZGO, Accompanied by Formation Energies[a] and Defect Energies[a] $\Delta E_{Zn,Ga,Cr}$ of Antisites (Zn_{Ga} or Ga_{Zn}) and of Cr in Defect-Free ZGO where Chromium Is Placed on a Zn or Ga Site

	ΔE^{s}_{form}	ΔE^{p}_{form}	$\Delta E^{s}_{Zn,Ga,Cr}$	$\Delta E^{p}_{Zn,Ga,Cr}$
ZGO	−197.737	−5.279	N.A.	N.A.
ZGO:Zn_{Ga}	−194.866	−4.126	2.871	1.153
ZGO:Ga_{Zn}	−197.486	−3.310	0.251	1.969
ZGO:Cr_{Zn}	−196.343	−1.832	1.393	3.447
ZGO:Cr_{Ga}	−197.984	−5.191	−0.247	0.088

[a]The quantities refer to the elemental solid (superscript s) or oxide precursor (superscript p) starting materials. All energies are given in eV and the formation energy is expressed for the entire 112-atom SC.

assumed starting materials. The formation energy represents the energy required to construct the entire compound from a given set of starting materials, and is calculated as

$$\Delta E_{form}[\text{ZGO: } X_Y] = E[\text{ZGO: } X_Y] - f(E_\alpha, E_\beta, E_O) \quad (1)$$

where X_Y is a Zn_{Ga} or a Ga_{Zn} antisite in the host, α and β are the starting materials, and f is a linear function with coefficients corresponding to the considered formation reaction. One can consider either the elemental solids (α = Zn, β = Ga) or the experimental oxide precursors (α = ZnO, β = Ga_2O_3) as starting materials, which leads to different values ΔE^{s}_{form} and ΔE^{p}_{form}, respectively (cf. Table 2). In particular, comparing the phase stability to the precursor materials gives a better approximation of the energetic position with respect to the so-called convex hull (i.e., the lowest obtainable energy for a given composition by linear combination of stable phases), leading to a more reliable energy picture.

Because the defect-free ZGO material is stable with respect to the used precursors ZnO and Ga_2O_3 (see Table 2), and therefore part of the convex hull of the ternary phase diagram, it is also interesting to express the defect stability with respect to this host. The defect energy, describing the stability of a defect against segregation, can be defined as

$$\Delta E_X = E[\text{host: } X_Y] - (E[\text{host}] + E[X] - E[Y]) \quad (2)$$

with X and Y indicative of the starting materials for the antisite defect energy, or equivalently:

$$\Delta E_X = \Delta E_{form}[\text{host: } X_Y] - \Delta E_{form}[\text{host}] \quad (3)$$

The same equations can be used for more general defects (see further). The reference energy of Zn and Ga (see eq 2) can again be expressed in terms of the elemental solids or the precursors, leading to different values of the defect energy and representing the stability against clustering of the elemental solids, ΔE^{s}_X, or the precursors, ΔE^{p}_X. For a given defect, both defect energies are related through the formation energy of the precursor materials out of the elemental solids (see Section S3 in the Supporting Information). Contrary to the formation energies in eq 1, defect energies directly express the stability of a defect in a host and are therefore used in the remainder of this work.

The combination of two antisites produces an antisite pair that, in the undoped ZGO, is characterized by the distance d_3 between the two sites (see Figure 2b). The corresponding defect energy is independent of the starting materials and is calculated as

$$\Delta E_{anti}(00d_3) = E[\text{host: } (00d_3)] - E[\text{host}] \quad (4)$$

with d_3 = 1, 2, or 3 corresponding to 3.50, 5.50, and 6.94 Å before relaxation, respectively (see Figure 2b). Figure 3 displays

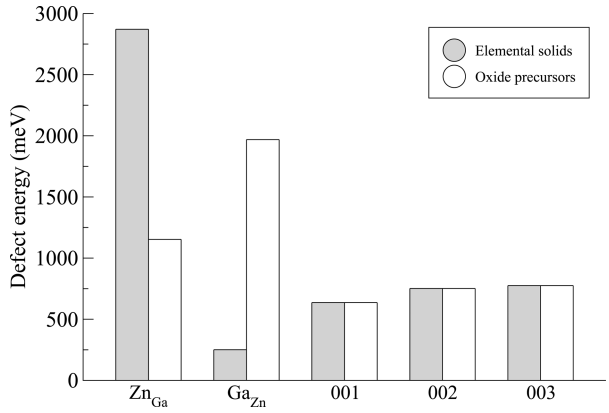

Figure 3. Calculated defect energies (in meV) of the various defects in the undoped ZGO host.

the calculated defect energies. The relative stability of the antisites depends on the starting materials, but in both cases an antisite pair is more stable than the mere combination of two single antisites. Figure 3 also shows that an antisite pair becomes less stable when the distance d_3 increases. This effect is relatively weak when the antisites are far from each other (i.e., comparing (002) with (003)) as the host itself also shields the charges (see Section 3.1.3).

3.1.3. Density of States and Charge Analysis. The defect energy describes the stability of the corresponding defect, but additional information on the occupation of the single-particle Kohn−Sham states and on the introduction of new states due to defects can be obtained from examining the density of states (DOS). It is incorrect to extract spectroscopic information from the DOS, as total energy differences between ground and excited states are needed for this.[21,34] When charge-transfer phenomena need to be addressed, be it shallow donor or acceptor behavior of defects, or charge-transfer luminescence originating from deep levels, the DOS is insufficient, and

DOI: 10.1021/acs.inorgchem.5b02805
Inorg. Chem. 2016, 55, 2402−2412

charge-state transition levels need to be calculated.[21,34,35] In this discussion, the DOS is solely exploited to acquire the electron occupation for various defects. All calculated DOS are included in Section S4 of the Supporting Information.

In Figure 4 the DOS is given for the ZGO host, ZGO containing an antisite, Zn_{Ga}, and ZGO containing an antisite pair ((001) configuration). It is found that a Zn_{Ga} antisite introduces two gap states, which are filled with approximately three out of four possible electrons when only this antisite is introduced. In case of Ga_{Zn}, no clear difference is found compared to ZGO, except that the Fermi level is raised due to the increased number of electrons (see Figure S2 in Supporting Information). The Fermi level for the Ga_{Zn} lies in the conduction band, and no clear localized character is observed, indicating that the extra electron is delocalized over the host. For the antisite pair configurations, it is found that both two-particle gap states resulting from the Zn_{Ga} inclusion are split in four one-particle states in case of a small d_3 distance (see Figure 4).

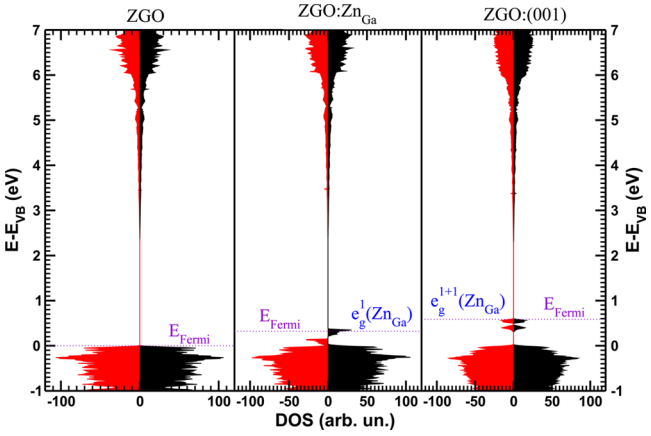

Figure 4. Calculated DOS of ZGO (left), ZGO:Zn_{Ga} (middle), and ZGO:(001) (right). Majority (red) and minority (black) spin are given in the left and right part of each DOS, respectively. The e_g states are indicated with their occupation in superscript.

To further rationalize the stability and charge compensation, atomic Hirshfeld-I charges were calculated (see Table 3 for charge differences taking the same-site Hirshfeld-I charges of the original ZGO host as a reference). The charge information on all configurations is included in Section S5 of the Supporting Information. Table 3 demonstrates that a Zn_{Ga} antisite is negatively charged (−0.295) compared to a Ga_{Ga} site in the original host. The small negative charge suggests that the Zn atom substituted at an octahedrally coordinated gallium site behaves almost as a gallium atom to maintain the bonding environment of the surrounding oxygens. This is also seen in the DOS where the e_g states are missing approximately one electron to obtain the d^{10} configuration. However, the transfer is not complete—as this would correspond to zero charge difference between the Zn_{Ga} and Ga_{Ga} site. In the same way, the oxygen atoms do not have the optimal amount of electrons resulting in a partial positive charge of +0.171 located mostly on the nearest neighbor shells of O (+0.119). The remaining charge is distributed mainly over the nearest neighbor shells of Ga and Zn atoms, respectively (+0.024 and +0.052). A Ga_{Zn} antisite behaves complementary, bearing a positive charge of +0.441 compared to a Zn_{Zn} site in the defect-free ZGO. The corresponding negative charge is spread out over mostly gallium (−0.248) and zinc (−0.171) as listed in Table 3. This charge is mostly located on the second cationic neighbor shells. In contrast to a Zn_{Ga} antisite, the creation of a Ga_{Zn} antisite barely affects the charge of the surrounding oxygen atoms.

In case of creation of an antisite pair, the negative charge of the Zn_{Ga} increases from −0.295 to −0.525 (see Table 3), nearly completely balancing the positive charge of the Ga_{Zn} antisite. The charge transfer brings both antisites closer to the d^{10} configuration and is the driving force for the stability of an antisite pair. Such a pair is indeed most stable when the sites of opposite charge are close to each other, explaining the stability ordering (001) > (002) ≈ (003) (see Figure 3). In addition, the interatomic distance between the antidefect sites appears to have little to no influence on the charge-transfer mechanism (compare the (001) and (003) configurations in Table S5 of the Supporting Information) in line with the observation that active sites in a system can have long-ranged charge interactions.[60]

3.2. Cr Doping of the Defect-Free ZGO Host.

Substitutional doping of ZGO with one chromium atom leads to two distinct doped ZGO materials, denoted as ZGO:Cr_{Zn} and ZGO:Cr_{Ga}.

3.2.1. Structural Properties. The local environments of the inserted chromium are shown in Figure 5. As the chromium

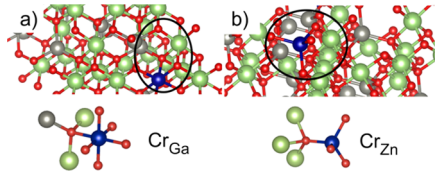

Figure 5. Surroundings of chromium on (a) a gallium or (b) a zinc position. Atoms are colored as follows: Zn, gray; Ga, green; Cr, blue; O, red.

Table 3. Differences of Atomic Hirshfeld-I Charges[a] for the Different Sites As Compared to the Charges on the Same Sites in ZGO

	ZGO:Zn_{Ga}	ZGO:Ga_{Zn}	ZGO:(001)	ZGO:Cr_{Ga}	ZGO:(100)	ZGO:(010)	ZGO:(111)
Zn_{Ga}	−0.295		−0.525		−0.499		−0.524
Ga_{Zn}		0.441	0.465			0.442	0.465
Cr_{Ga}				0.145	0.384	0.146	0.147
Zn	0.077	−0.193	0.006	0.009	0.059	−0.189	0.013
Ga	0.046	−0.248	0.054	−0.016	0.030	−0.263	0.031
O	0.171	−0.0004	−0.003	−0.138	0.021	−0.138	−0.136

[a]The values of Zn, Ga, and O are the sum of all relative charges of atoms of this kind. In line with the Kröger−Vink notation, charges of the same sites in the host were compared throughout the paper.

DOI: 10.1021/acs.inorgchem.5b02805
Inorg. Chem. 2016, 55, 2402−2412

atom is almost of equal size compared to the original Ga and Zn atoms,[61] the bond lengths in the immediate vicinity do not vary much. The difference in bond length is only −0.5% and +0.5% for doping on a Ga and Zn position, respectively, and all distances to the nearest neighbors change equally. The average Cr−O distance of 1.98 Å for Cr_{Ga} is in good agreement with the experimental value of 1.96 Å, obtained using EXAFS spectroscopy as recently reported by Basavaraju et al.[62]

3.2.2. Stability Analysis. The stability of the ZGO:Cr_{Zn} and ZGO:Cr_{Ga} materials can again be characterized using both the formation and defect energy (see Table 2). The formation energy is now calculated as

$$\Delta E_{form}[\text{ZGO: Cr}_X] = E[\text{ZGO: Cr}_X] - f(E_\alpha, E_\beta, E_\gamma, E_O) \quad (5)$$

where X is a Zn or Ga, and α, β, and γ define the starting materials. One can again consider the elemental solids (α = Zn, β = Ga, γ = Cr) or the experimental precursors (α = ZnO, β = Ga_2O_3, γ = Cr_2O_3) as starting materials (ΔE^s_{form} and ΔE^p_{form}, cf. Table 2). The defect energy ΔE_{Cr}—in this case also referred to as the dopant energy—now describes the stability of the Cr dopant in the host compared to its native environment (ΔE^s_{Cr} or ΔE^p_{Cr}, cf. Table 2) and is calculated with eq 2, where X is Cr, and Y can be Zn or Ga. It expresses the stability of the dopant against segregation of a chromium phase. Table 2 shows that the increased stability of the precursor materials with respect to the elemental solids translates in a decreased stability when going from ΔE^s_{form} to ΔE^p_{form}. For the same reason, the stability of the defect-free ZGO causes defect energies to be higher than formation energies. Nevertheless, all studied quantities yield the same qualitative picture, that is, that Cr_{Ga} is energetically more favorable than Cr_{Zn}. Even Cr_{Ga} has a slightly positive energy compared to the convex hull of the quaternary phase diagram, as evidenced by ΔE^p_{Cr}, but the energy difference per atom is small (only 88 meV/unit cell, see Table 2) and can be compensated by finite-temperature effects.

3.2.3. Density of States. Figure 6 displays the calculated DOS for the ZGO host and for the two Cr-doped materials. It can be seen that the chromium dopant introduces additional energy levels in the band gap of the ZGO host. The obtained single-particle splitting in t_2/t_{2g} and e/e_g orbitals is qualitatively in line with the tetrahedral or octahedral surrounding (see Figure 5) obtained for substitution on a Zn or Ga position, respectively. The DOS of ZGO:Cr_{Zn} indicates two fully occupied lower-lying e levels and two occupied and one unoccupied higher-lying t_2 levels. Hence, DFT predicts a $3d^4$ configuration for the ZGO:Cr_{Zn} defect, which is spectroscopically known as Cr^{2+}. This configuration has a completely different fingerprint than the more common $3d^3$ configuration in Cr^{3+}. Cr^{2+} luminescence is known to occur in multiple II−VI semiconductors and features infrared emission in the range of 2−2.5 μm.[63−66] In contrast, the DOS of ZGO:CrGa contains three occupied t_{2g} levels and two unoccupied, higher-lying e_g levels. Hence, for ZGO:Cr_{Ga}, a $3d^3$ configuration is predicted.

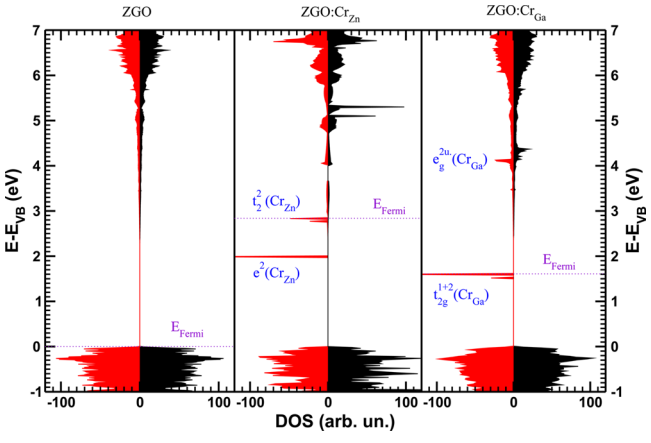

Figure 6. Calculated DOS of ZGO (left), ZGO:Cr_{Zn} (middle), and ZGO:Cr_{Ga}(right). Majority (red) and minority (black) spin are given in the left and right part of each DOS. The t_2/t_{2g} and e/e_g states are indicated with their occupation in superscript.

3.3. Single Antisites in the Doped ZGO Host. In this section, the influence of isolated antisites in the doped ZGO:Cr material is studied. Only the most stable doped configuration is considered, with the Cr^{3+} ion at a Ga position (see Section 3.2). Contrary to the antisites in the undoped ZGO host, different antisite configurations now arise due to a varying distance of the antisite to the chromium dopant. The configurations are therefore labeled using the relevant distance between the antisite and the chromium dopant, being d_1 or d_2 as defined in Figure 2. In the case of Zn_{Ga} this leads to five potential structures ($d_1$00), whereas three for Ga_{Zn} are indicated by (0$d_2$0). There are more antisite configurations for Zn_{Ga} because there are more gallium atoms in ZGO, making more locations accessible around the chromium atom than for Ga_{Zn}.

3.3.1. Structural Properties. In line with the observations for antisites in the undoped material (Section 3.1.1), the structural properties of the defect-containing doped materials differ significantly from those of the initial ZGO host. For Zn_{Ga}, the average distance to the nearest oxygen neighbors increases from 2.02 to 2.12 Å, which is comparable with ZGO:Zn_{Ga} (2.08 Å). The (100) configuration is the sole exception, since not all distances change in the same way: the average distance to the four equatorial oxygen atoms changes from 2.02 to 2.06 Å, whereas the distance to the two axial oxygen atoms increases from 2.02 to 2.23 Å, yielding a slightly elongated octahedron around the Zn_{Ga}. For Ga_{Zn}, all distances change in the same way from 2.02 to 2.12 Å, similar to the Ga_{Zn} defect in undoped ZGO.

Next, we examine the local environment of the chromium dopant and its distortion due to inclusion of antisites. In the ZGO:Cr_{Ga} material, the dopant sits in a slightly distorted octahedral environment as shown in detail in Figure 7. All calculated angles are included in Section S6 of the Supporting

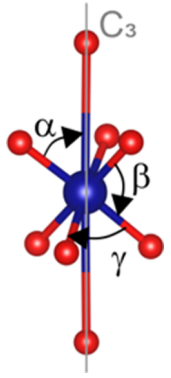

Figure 7. Detailed view of the local chromium environment when substituted on a Ga site. The C_3 axis is indicated, as well as relevant angles α, β, and γ.

DOI: 10.1021/acs.inorgchem.5b02805
Inorg. Chem. 2016, 55, 2402−2412

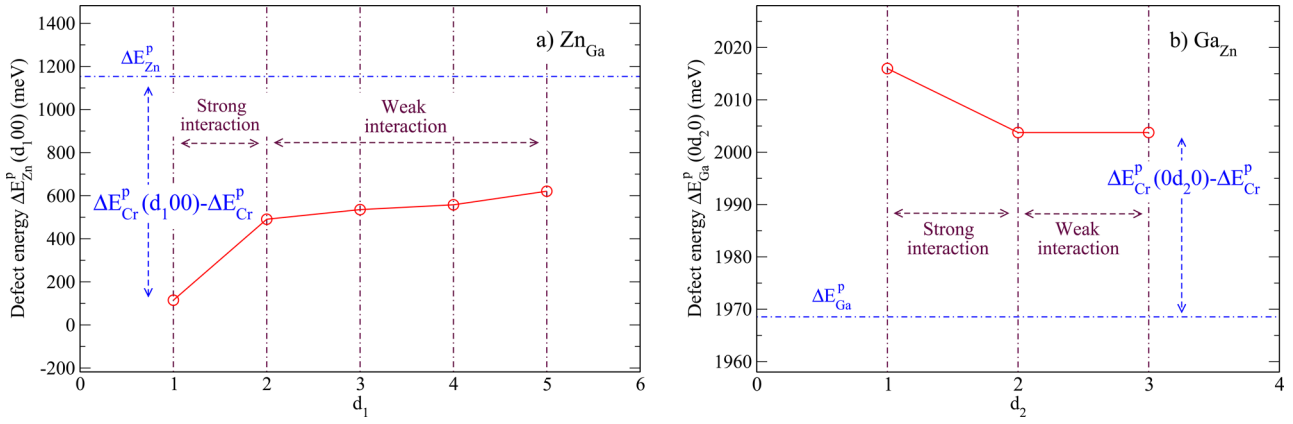

Figure 8. Defect energies for all configurations of the single substitutional (a) Zn_{Ga} and (b) Ga_{Zn} defects in ZGO:Cr_{Ga}. The defect energies in the undoped ZGO host are indicated with blue dotted lines.

Information. The angle α between the Cr−O bonds and the C_3 axis (formed using the second nearest oxygen neighbors) equals 50.8°. This should be compared with the experimental value of 53.4° reported by Gourier et al. for the chromium ion in the unperturbed case (denoted as Cr_α also seen in Table. 1).[14] Introduction of a Ga_{Zn} antisite only minorly perturbs the local chromium environment. A maximal change of 1.5° is found for β in case of the (010) configuration. This small distortion even decreases when the antisite is located further from the Cr dopant. The situation is altered in case of introduction of a Zn_{Ga} antisite, as the theoretical data indicate that the local Cr environment is severely distorted for the (100) and (200) configurations. For the (100) configuration, where the Zn_{Ga} antisite is positioned at only 3.0 Å from the Cr dopant, α and γ differ with 4.6° and 11.6° from the defect-free ZGO:Cr. A similar distortion is found for (200). For Zn_{Ga} at larger distance, the distortion of the Cr environment is reduced; for example, γ differs only 2.2° from the unperturbed situation in case of the (300) configuration.

3.3.2. Stability Analysis. The defect energy of single antisite defects in ZGO:Cr is calculated from eq 2. The combination of the Cr dopant and an antisite defect moreover allows to calculate the stability of the Cr dopant, with regard to the defect-containing material. The resulting dopant and defect energies are related; for example, for the Zn_{Ga} defect in the Cr-doped material we obtain

$$\Delta E_{Cr}(d_1 00) - \Delta E_{Cr} = \Delta E_{Zn}(d_1 00) - \Delta E_{Zn} \quad (6)$$

Indeed, there is a special relation between defect energies when two defects are present in a host material:

$$\Delta E_1[\text{host: } 1, 2] - \Delta E_1[\text{host: } 1] = \Delta E_2[\text{host: } 1, 2] - \Delta E_2[\text{host: } 2] \quad (7)$$

Equation 7 represents the mutual interaction between two defects in a host material and states that the influence of the first defect on the defect energy of a second one is equal to the influence of the second defect on the defect energy of the first one.

Figure 8a displays the calculated defect energies of the five configurations for the Zn_{Ga} antisite. The lowest defect energy, corresponding to a decreased instability, is found for the (100) configuration, that is, when the antisite is close to the chromium atom. In line with eq 6, this stabilization of Zn_{Ga} in the presence of Cr (shown by the position of the red curve with respect to the blue curve in Figure 8a) also means that the chromium dopant is stabilized by the presence of the antisite. This trend is explained by the charge transfer between the dopant and the defect. In case of Zn_{Ga} the energy levels of Zn_{Ga} are lower than the levels of the chromium atom (see the DOS in Figures 4 and 6), and hence an electron is transferred to the defect to achieve a stable d^{10} configuration. This transfer, albeit incomplete (see Hirshfeld-I charges in Section 3.3.3), would suggest the formation of a $Cr^{4+}(d^2)$ configuration, which is not observed experimentally, and thus the occurrence of a single Zn_{Ga} defect in the Cr-doped material is not expected.

In contrast, Figure 8b reveals that an increasing distance between the chromium atom and Ga_{Zn} only weakly reduces its instability. In this case, the defect energy $\Delta E_{Ga}(0d_2 0)$ is less affected by changing d_2 than $\Delta E_{Zn}(d_1 00)$ is affected by changing d_1, and the addition of the Cr atom does not cause a large energy variation of the defect (Figure 8b). These findings are also supported by the DOS and the calculated Hirshfeld-I charges (see Section 3.3.3).

Both antisites have an opposite preferable configuration with respect to their distance to the chromium atom. Importantly, the antisites in ZGO:Cr are still unstable and are hence not expected to exist.

3.3.3. Density of States and Charge Analysis. The interaction between the defect and the chromium atom as a function of their distance is also examined by calculating the DOS for the distinct configurations. All calculated DOS are included in the Supporting Information (Section S7). In Figure 9 the projected density of states (PDOS) on the d-orbitals of the chromium atom is illustrated for two Zn_{Ga} defects in ZGO:Cr. The strong interaction between the Zn_{Ga} defect and chromium dopant at close distance (i.e., the (100) configuration) induces an extra splitting of the t_{2g} levels, which now contain approximately two electrons because of the transfer to the defect. When the defect is located further from the chromium atom (i.e., the (300) configuration) the interaction between dopant and defect weakens, and these levels rejoin. Compared to ZGO:Cr_{Ga}, the minority t_{2g} levels levels are now below the minority e_g levels due to interaction with the Zn_{Ga}, resulting in three clearly split unoccupied t_{2g} peaks in Figure 9. This behavior is independent of the distance d_1 and therefore most likely caused by the changed occupation of the chromium atom from t_{2g}^3 to t_{2g}^2. For the Ga_{Zn} defect no substantial interaction between the chromium atom and the defect is observed, irrespective of their distance (see Figure S6 in the

DOI: 10.1021/acs.inorgchem.5b02805
Inorg. Chem. 2016, 55, 2402−2412

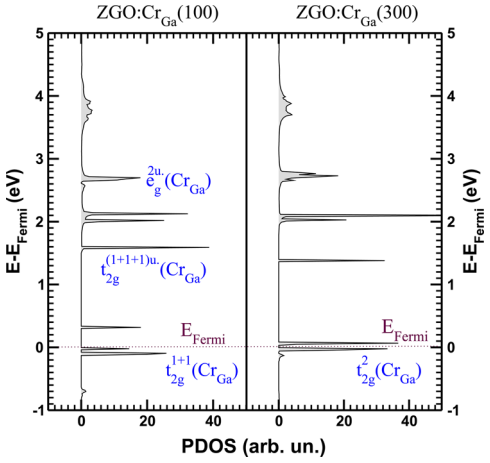

Figure 9. PDOS on the d-orbitals of the chromium atom with ZGO:(100) (left) and ZGO:(300) (right). These PDOS clearly indicate the splitting of the occupied t_{2g}(Cr) levels when the distance between Zn_{Ga} and Cr_{Ga} is small.

Supporting Information). This observation is in line with the conclusion based on the defect energies that the interaction between the Ga_{Zn} defect and chromium dopant is very small (see Section 3.3.2).

Analysis of the atomic Hirshfeld-I charges indicates that a Zn_{Ga} antisite becomes more negative (from −0.295 to −0.499), whereas the positive charge on the chromium atom correspondingly increases from 0.145 to 0.385 (e.g., configuration (100), Table 3). These results confirm the charge transfer. The driving force of this electron transfer is the stabilization of the Zn_{Ga} to create the d^{10} configuration. The most stable configuration is achieved when the created opposite charges are close to each other, that is, configuration (100).

3.4. Antisite Pairs in the Doped Material. In this final section, antisite pairs are examined in ZGO:Cr. For these configurations, the distance d_3 is also varied, similar to the analysis performed in Section 3.1.

3.4.1. Structural Properties. Table 4 lists for all investigated ($d_1d_2d_3$) configurations the relevant optimized bond lengths. It is seen that for all 30 configurations these optimized values are close to the initial distances (Figure 2b). The largest changes upon optimization are found for the (d_1d_21) configurations with a maximal change in bond length of 0.04 Å (1.1%).

The influence of introducing an antisite pair on the local Cr environment (see Table S8 in the Supporting Information) is examined. The distorted octahedral environment (Figure 7) is mainly affected by the presence of the Zn_{Ga}, and d_1 dominates the overall behavior. For all configurations with $d_1 = 1$ the local Cr environment is substantially distorted. In particular, γ changes with ∼5° from the angle in ZGO:Cr, whereas for $d_1 = 3$ this distortion is severely reduced (e.g., changes in γ are below 1°). Moreover, increasing d_3 also results in a reduction of the distortion as shown by comparing (121), (122), and (123). These findings are again in line with the structural behavior previously proposed by Gourier et al. based on experimental EPR measurements. These authors reported three antisite pair configurations with Zn_{Ga} in the first cationic coordination (denoted as $Cr_{\gamma,\delta,\epsilon}$, see Table 1) that contribute to the N2 line and for which the distortion indeed decreases with increasing distance between the antisites (i.e., increasing d_3).[14] Our simulated data support these experimental findings and moreover indicate that a variety of configurations should be considered to contribute to the N2 line.

3.4.2. Stability Analysis. To investigate the stability of the materials combining a Cr dopant and an antisite pair, the following quantities are employed:

$$\Delta E_{anti}(d_1d_2d_3) = E[\text{ZGO: } Cr_{Ga}(d_1d_2d_3)] - E[\text{ZGO: } Cr_{Ga}] \quad (8)$$

$$\Delta E_{Cr}(d_1d_2d_3) = E[\text{ZGO: } Cr_{Ga}(d_1d_2d_3)] - (E[\text{ZGO: } (00d_3)] - E[\text{Ga}] + E[\text{Cr}]) \quad (9)$$

The first value represents the stability of the antisite pair in ZGO:Cr, whereas the second represents the stability of the Cr dopant in ZGO containing an antisite pair. The relation between the different defect energies is schematically shown in Figure 10. It is seen that (example of eq 7)

$$\Delta E^{s}_{Cr}(d_1d_2d_3) = \Delta E_{anti}(d_1d_2d_3) + \Delta E^{s}_{Cr} - \Delta E_{anti}(00d_3) \quad (10)$$

Table 4. Relevant Interatomic Distances[a] $d_1 = d(Zn_{Ga}–Cr_{Ga})$, $d_2 = d(Ga_{Zn}–Cr_{Ga})$, and $d_3 = d(Zn_{Ga}–Ga_{Zn})$

$d_1d_2d_3$	d_1	d_2	d_3	ΔE^{rel}_{form}	$d_1d_2d_3$	d_1	d_2	d_3	ΔE^{rel}_{form}
111	2.97	3.51	3.52	25	**312**	5.97	3.49	5.50	119
112	2.98	3.49	5.48	135	**313**	5.99	3.50	6.94	148
121	2.97	5.51	3.54	18	**321**	5.97	5.49	3.53	0
122	2.99	5.49	5.50	135	**322**	5.98	5.50	5.50	117
123	2.98	5.51	6.93	158	**323**	5.99	5.50	6.94	139
132	2.98	6.94	5.50	136	**331**	5.99	6.94	3.53	3
133	2.98	6.93	6.94	159	**332**	5.98	6.93	5.50	116
211	5.19	3.49	3.53	10	**411**	6.70	3.50	3.54	12
212	5.20	3.49	5.51	127	**412**	6.69	3.50	5.50	124
213	5.18	3.50	6.93	150	**413**	6.69	3.50	6.94	149
221	5.20	5.49	3.53	5	**421**	6.67	5.51	3.53	4
223	5.18	5.50	6.94	144	**422**	6.68	5.51	5.50	119
231	5.17	6.92	3.53	6	**431**	6.69	6.92	3.51	5
232	5.18	6.93	5.50	121	**512**	8.45	3.51	5.50	129
311	5.97	3.50	3.54	8	**521**	8.44	5.49	3.53	7

[a]In angstroms, as defined in Figure 2 for all configurations combining the Cr dopant with an antisite pair. Formation energy differences ΔE^{rel}_{form}, relative to the most stable configuration, are also given (in meV/unit cell).

DOI: 10.1021/acs.inorgchem.5b02805
Inorg. Chem. 2016, 55, 2402−2412

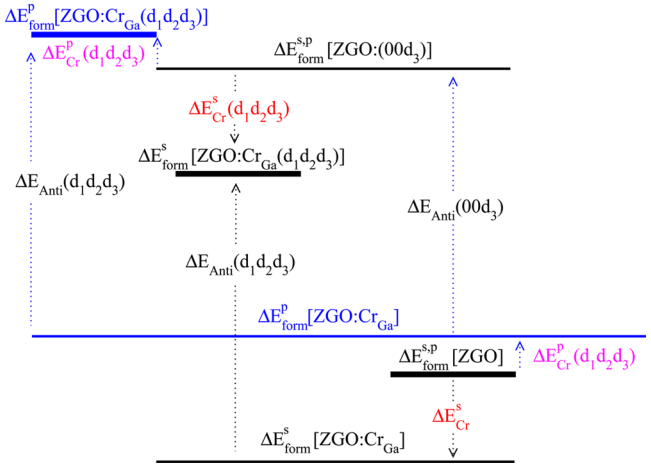

Figure 10. Schematic representation of the relation between the various dopant and defect energies in ZGO. The antisite defect energies (in black) are independent of the starting materials, whereas for the Cr dopant energy the oxide precursors (in pink) or elemental solids (in red) can be taken.

from which we conclude that, for fixed d_3, $\Delta E_{anti}(d_1d_2d_3)$ and $\Delta E^s_{Cr}(d_1d_2d_3)$ follow the same trend as a function of d_1 and/or d_2. The generated energy scheme of Figure 10 schematically links the different elements and elucidates the interplay between the dopant and defects. All calculated values are included in Table S9 in the Supporting Information. It can overall be noted that the presence of the Cr dopant only minorly affects the calculated antisite defect energies, and vice versa, the inclusion of an antisite pair has little influence on the calculated Cr dopant energy.

Figure 11 displays the $\Delta E_{anti}(d_1d_2d_3)$ defect energies for the twelve (d_1d_21) and seven (d_1d_23) antisite pairs around the chromium. Comparison between both graphs indicates that the antisites attract each other, as evidenced by the increased stability of the configurations with short d_3 distance. As for the undoped ZGO (Section 3.1), this behavior is again due to a charge transfer between the two antisites. The attractive interaction between both antisites is most pronounced if the sites of opposite charge are close to each other, that is, ~3.5 Å. Figure 11 also reveals that the same general behavior, that is, a minimum defect energy as a function of the Zn_{Ga} d_1 distance (and in particular at $d_1 = 3$). It is moreover seen that there is also a minimum for the Ga_{Zn}−Cr_{Ga} d_2 distance, in particular, at $d_2 = 2$. Hence, the minimum energy is found for a defect configuration that combines these two distances, that is, configuration (321) (see also Table 4). Notably, the relative energies of all 30 configurations combining a dopant and antisite pair vary only within a 160 meV range (as seen from ΔE^{rel}_{form} in Table 4). Clearly, the configurations with small d_3 distance are favored, as they all lie within a very narrow energy range of only 18 meV with respect to the most stable (321) configuration.

3.4.3. Density of States and Charge Analysis. In Figure 12 the DOS is plotted for four antisite pair configurations in ZGO:Cr. In the first configuration (111) all sites of interest (i.e., both antisites and the chromium dopant) are very close to each other. In the subsequent DOS the different parts are put further from each other, resulting in the (311), (321), and (322) configurations. An increase in d_1 mainly affects the t_{2g} levels of the chromium dopant, whereas an increase in d_2 has little influence on the overall DOS. Finally, an increase in d_3 means that the e_g levels of the Zn_{Ga} rejoin.

In Table 3 the changes in atomic Hirshfeld-I charges are also listed for the (111) configuration (data of other configurations are included in section S5 of the Supporting Information). In contrast to the introduction of a single Zn_{Ga} antisite (e.g., configuration (100)), no charge is transferred between the chromium and the Zn_{Ga} antisite. Instead, a charge transfer between both antisites occurs similar to the situation of an antisite pair in the Cr-defect-free host. No major difference is seen between the different configurations, suggesting that the energy is largely dominated by the distances between the two antisites of opposite charge. This is in correspondence with previous experimental observations where only typical Cr^{3+} luminescence, that is, luminescence originating from a $3d^3$ configuration, is found.[11−19] The combination of Kohn−Sham DFT calculations and optical spectroscopy therefore shows that antisite defects only occur in Zn_{Ga}−Ga_{Zn} pairs. When these are close to the luminescent Cr_{Ga} center, the local point symmetry and bond lengths change, yielding emission at slightly different wavelengths.

4. CONCLUSIONS

This work investigated the behavior of antisite defect configurations in the chromium-doped zinc gallate (ZGO:Cr) by means of DFT simulations of large supercells. This

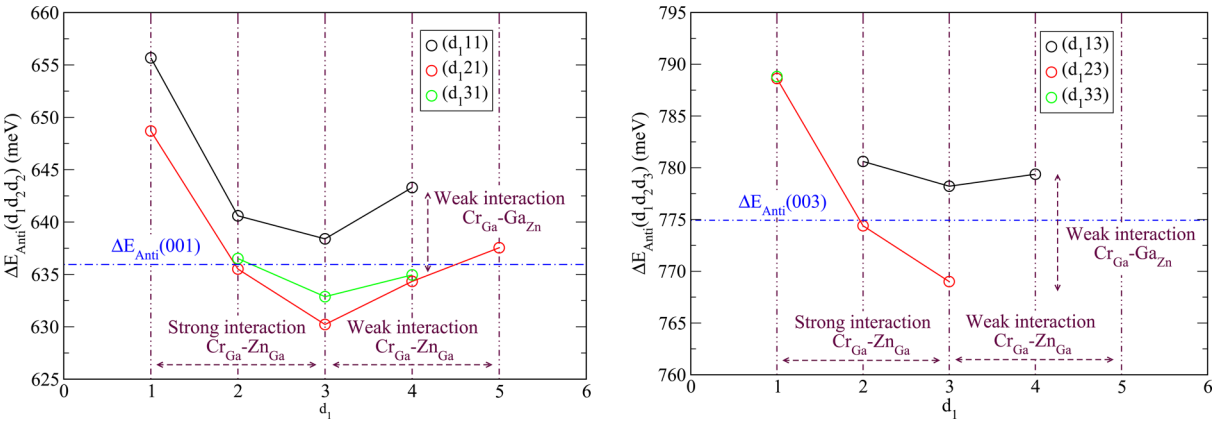

Figure 11. Antisite defect energies $\Delta E_{anti}(d_1d_2d_3)$ in the doped material. The defect energies ΔE_{anti} in the undoped ZGO host are indicated with blue dotted lines.

DOI: 10.1021/acs.inorgchem.5b02805
Inorg. Chem. 2016, 55, 2402−2412

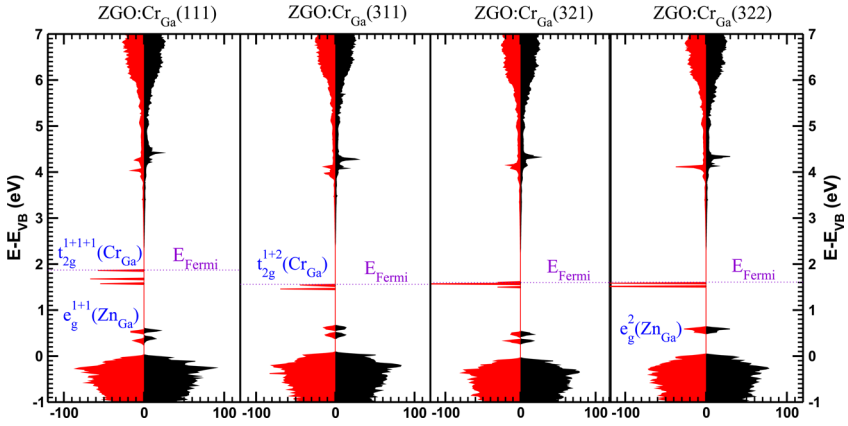

Figure 12. Calculated DOS of various configurations containing a chromium dopant and antisite defect pair. (left to right) An antisite defect site is put further away from Cr (going from (111) over (311) to (321)), and in the last plot (configuration (322)) both antisite defect sites are put farther from each other. Majority (red) and minority (black) spin are given in the left and right part of each DOS. The t_{2g} and e_g states are indicated with their occupation in superscript.

theoretical characterization provides detailed atomic-scale information on the local structural distortions and stability of these complex materials. Various configurations of isolated antisites, Zn_{Ga} or Ga_{Zn}, and antisite pairs have been studied in undoped as well as chromium-doped ZGO.

The calculated dopant energies showed that, in line with experimental observations, the luminescent chromium dopant is preferably situated at a slightly distorted octahedrally coordinated gallium site. The chromium substitution introduces three occupied t_{2g} levels in the band gap of ZGO. Isolated antisites were found to be unstable in undoped ZGO. However, simultaneous insertion of two antisites, that is, the formation of an antisite pair, increased the stability substantially as demonstrated using calculated defect energies. This stability was further rationalized by analysis of calculated Hirshfeld-I charges and the density of states (DOS), revealing a charge transfer from Ga_{Zn} to Zn_{Ga} aiming to restore the d^{10} configuration on both antisites. This charge transfer causes both antisites of the pair to be as close as possible to compensate each other's charge.

Inserting antisites in ZGO:Cr indicated that mainly the Zn_{Ga} antisite interacts with the chromium atom, causing a severe distortion of the local Cr environment. Moreover, the Cr energy levels split further when Zn_{Ga} was located near the dopant. The Ga_{Zn} however only minorly distorted the local Cr environment, did not introduce gap states, and had no effect on the chromium state. Introducing an antisite pair in the chromium-doped ZGO resulted again in the creation of opposite charges on both antisites, yielding a stable $3d^3$ configuration for the Cr atom in all investigated defect cluster geometries. The configuration is most stable when the two antisites are close to each other (i.e., ∼3.5 Å). It was found that this interplay between both antisites, dominates the overall stability picture of a ZGO combining a dopant and antisite pair. These insights agree with previous experimental findings of Gourier et al.[13,14] and Allix et al.[19] on the responsible structures in the persistent luminescent mechanism. Hence our DFT calculations underpin the possibility that an antisite defect pair is formed in the first coordination shells of the Cr dopant, influencing the Cr emission spectrum and possibly being responsible for the charge trapping at the origin of the delayed luminescence.

This work demonstrates that theoretical simulations combining the analysis of energies, DOS, and charges, can provide clear qualitative trends in the geometrical and energetical behavior of a series of dopant-defect configurations. As a result, antisite defect configurations of ZGO:Cr can be selected for further analysis of their luminescent characteristics. In view of the overall importance of defect-containing spinel materials for optical applications, theoretical simulations offer a viable alternative to gain information on the behavior at the atomic scale.

■ ASSOCIATED CONTENT

Supporting Information

The Supporting Information is available free of charge on the ACS Publications website at DOI: 10.1021/acs.inorgchem.5b02805.

Comparison of experimental and theoretical geometrical parameters; influence of the cell size; relation between defect and formation energies; density of states in the undoped ZGO host; atomic Hirshfeld-I charges; local chromium environment; density of states in the chromium-doped ZGO host; defect energies of the ZGO configurations combining a chromium dopant and antisite pair. (PDF)

■ AUTHOR INFORMATION

Corresponding Authors

*E-mail: Philippe.Smet@UGent.be. (P.F.S.)
*E-mail: Karen.Hemelsoet@UGent.be. (K.H.)

Notes

The authors declare no competing financial interest.

■ ACKNOWLEDGMENTS

The Fund for Scientific Research-Flanders (FWO), the Research Board of Ghent Univ. (BOF), and BELSPO in the frame of IAP-PAI P7/05 are acknowledged for their financial support. D.E.P.V. is a postdoctoral researcher funded by the FWO (Project No. 12S3415N). Computational resources and services were provided by the Stevin Supercomputer Infrastructure of Ghent Univ. and by the Flemish Supercomputer Center (VSC), funded by the Hercules Foundation and the Flemish Government—Department EWI.

DOI: 10.1021/acs.inorgchem.5b02805
Inorg. Chem. 2016, 55, 2402−2412

REFERENCES

(1) Van den Eeckhout, K.; Smet, P. F.; Poelman, D. *Materials* **2010**, *3*, 2536−2566.
(2) Brito, H. F.; Hölsä, J.; Laamanen, T.; Lastusaari, M.; Malkamäki, M.; Rodrigues, L. C. V. *Opt. Mater. Express* **2012**, *2*, 371−381.
(3) Smet, P. F.; Poelman, D.; Hehlen, M. P. *Opt. Mater. Express* **2012**, *2*, 452−454.
(4) Van den Eeckhout, K.; Poelman, D.; Smet, P. F. *Materials* **2013**, *6*, 2789−2818.
(5) Matsuzawa, T.; Aoki, Y.; Takeuchi, N.; Murayama, Y. *J. Electrochem. Soc.* **1996**, *143*, 2670−2673.
(6) Korthout, K.; Van den Eeckhout, K.; Botterman, J.; Nikitenko, S.; Poelman, D.; Smet, P. F. *Phys. Rev. B: Condens. Matter Mater. Phys.* **2011**, *84*, 085140.
(7) Zhuang, Y.; Katayama, Y.; Ueda, J.; Tanabe, S. *Opt. Mater.* **2014**, *36*, 1907−1912.
(8) Liu, F.; Yan, W. Z.; Chuang, Y. J.; Zhen, Z. P.; Xie, J.; Pan, Z. W. *Sci. Rep.* **2013**, *3*, 1554.
(9) Xu, J.; Ueda, J.; Tanabe, S. *Opt. Mater. Express* **2015**, *5*, 963−968.
(10) Pan, Z.; Lu, Y.-Y.; Liu, F. *Nat. Mater.* **2011**, *11*, 58−63.
(11) Bessière, A.; Jacquart, S.; Priolkar, K.; Lecointre, A.; Viana, B.; Gourier, D. *Opt. Express* **2011**, *19*, 10131−10137.
(12) Maldiney, T.; Richard, C.; Sherman, D.; Gourier, D.; Viana, B.; Bessière, A. Nanoparticules a luminescence persistante excitable in situ pour l'imagerie optique in vivo, l'imagerie multimodale optique-IRM in vivo et la theranostique. Patent 2014037157.
(13) Bessière, A.; Sharma, S. K.; Basavaraju, N.; Priolkar, K. R.; Binet, L.; Viana, B.; Bos, A. J. J.; Maldiney, T.; Richard, C.; Scherman, D.; Gourier, D. *Chem. Mater.* **2014**, *26*, 1365−1373.
(14) Gourier, D.; Bessière, A.; Sharma, S.; Binet, L.; Viana, B.; Basavaraju, N.; Priolkar, K. R. *J. Phys. Chem. Solids* **2014**, *75*, 826−837.
(15) Maldiney, T.; Bessière, A.; Seguin, J.; Teston, E.; Sharma, S. K.; Viana, B.; Bos, A. J. J.; Dorenbos, P.; Bessodes, M.; Gourier, D.; Scherman, D.; Richard, C. *Nat. Mater.* **2014**, *13*, 418−426.
(16) Sharma, S. K.; Bessière, A.; Basavaraju, N.; Priolkar, K. R.; Binet, L.; Viana, B.; Gourier, D. *J. Lumin.* **2014**, *155*, 251−256.
(17) Sharma, S.; Gourier, D.; Viana, B.; Maldiney, T.; Teston, E.; Scherman, D.; Richard, C. *Opt. Mater.* **2014**, *36*, 1901−1906.
(18) Basavaraju, N.; Priolkar, K. R.; Gourier, D.; Sharma, S. K.; Bessière, A.; Viana, B. *Phys. Chem. Chem. Phys.* **2015**, *17*, 1790−1799.
(19) Allix, M.; Chenu, S.; Veron, E.; Poumeyrol, T.; Kouadri-Boudjelthia, E. A.; Alahrache, S.; Porcher, F.; Massiat, D.; et al. *Chem. Mater.* **2013**, *25*, 1600−1606.
(20) Hölsä, J. *Electrochem. Soc. Interface* **2009**, 42−45.
(21) Joos, J. J.; Poelman, D.; Smet, P. F. *Phys. Chem. Chem. Phys.* **2015**, *17*, 19058−19078.
(22) Atanasov, M.; Ganyushin, D.; Sivalingam, K.; Neese, F. *Struct. Bonding* **2011**, *143*, 149−220.
(23) Barandiaran, Z.; Seijo, L. *J. Chem. Phys.* **2013**, *138*, 074102.
(24) Seijo, L.; Barandiaran, Z. *Phys. Chem. Chem. Phys.* **2013**, *15*, 19221−19231.
(25) Seijo, L.; Barandiaran, Z. *Opt. Mater.* **2013**, *35*, 1932−1940.
(26) Zhai, D. Y.; Ning, L. X.; Huang, Y. C.; Liu, G. K. *J. Phys. Chem. C* **2014**, *118*, 16051−16059.
(27) Seijo, L.; Barandiaran, Z. *Phys. Chem. Chem. Phys.* **2014**, *16*, 3830−3834.
(28) Krosnicki, M.; Kedziorski, A.; Seijo, L.; Barandiaran, Z. *J. Phys. Chem. A* **2014**, *118*, 358−368.
(29) Pascual, J. L.; Barandiaran, Z.; Seijo, L. *J. Lumin.* **2014**, *145*, 808−817.
(30) Lejaeghere, K.; Van Speybroeck, V.; Van Oost, G.; Cottenier, S. *Crit. Rev. Solid State Mater. Sci.* **2014**, *39*, 1−24.
(31) Du, M. H. *ECS J. Solid State Sci. Technol.* **2016**, *5*, 12.
(32) Du, M. H. *J. Mater. Chem. C* **2014**, *2*, 2475.
(33) Du, M. H. *J. Lumin.* **2015**, *157*, 69−73.
(34) Freysoldt, C.; Grabowski, B.; Hickel, T.; Neugebauer, J.; Kresse, G.; Janotti, A.; Van de Walle, C. G. *Rev. Mod. Phys.* **2014**, *86*, 253−305.
(35) Dixit, H.; Tandon, N.; Cottenier, S.; Saniz, R.; Lamoen, D.; Partoens, B. *Phys. Rev. B: Condens. Matter Mater. Phys.* **2013**, *87*, 174101.
(36) Assali, L. V. C.; Machado, W. V. M.; Justo, J. F. *Phys. Rev. B: Condens. Matter Mater. Phys.* **2004**, *69*, 155212.
(37) Assali, L. V. C.; Machado, W. V. M.; Justo, J. F. *Phys. Rev. B: Condens. Matter Mater. Phys.* **2011**, *84*, 155205.
(38) Benecha, E. M.; Lombardi, E. B. *Phys. Rev. B: Condens. Matter Mater. Phys.* **2011**, *84*, 235201.
(39) Munoz-Garcia, A. B.; Artacho, E.; Seijo, L. *Phys. Rev. B: Condens. Matter Mater. Phys.* **2009**, *80*, 014105.
(40) Munoz-Garcia, A. B.; Seijo, L. *J. Phys. Chem. A* **2011**, *115*, 815−823.
(41) Munoz-Garcia, A. B.; Barandiaran, Z.; Seijo, L. *J. Mater. Chem.* **2012**, *22*, 19888−19897.
(42) Sham, L. J.; Schlüter, M. *Phys. Rev. Lett.* **1983**, *51*, 1888−1891.
(43) Perdew, J. *Int. J. Quantum Chem.* **1985**, *28*, 497.
(44) Godby, R. W.; Schluter, M.; Sham, L. J. *Phys. Rev. Lett.* **1986**, *56*, 2415.
(45) Mori-Sanchez, P.; Cohen, A. J.; Yang, W. *Phys. Rev. Lett.* **2008**, *100*, 146401.
(46) Anisimov, V. I.; Aryasetiawan, F.; Lichtenstein, A. I. *J. Phys.: Condens. Matter* **1997**, *9*, 767−808.
(47) Heyd, J.; Scuseria, G. E.; Ernzerhof, M. *J. Chem. Phys.* **2003**, *118*, 8207−8215.
(48) Hedin, L. *Phys. Rev.* **1965**, *139*, A796.
(49) Dixit, H.; Tandon, N.; Cottenier, S.; Saniz, R.; Lamoen, D.; Partoens, B.; Van Speybroeck, V.; Waroquier, M. *New J. Phys.* **2011**, *13*, 063002.
(50) Kresse, G.; Furthmüller, J. *Comput. Mater. Sci.* **1996**, *6*, 15.
(51) Hafner, J. *J. Comput. Chem.* **2008**, *29*, 2044−2078.
(52) Perdew, J. P.; Burke, K.; Ernzerhof, M. *Phys. Rev. Lett.* **1996**, *77*, 3865−3868.
(53) Blöchl, P. E. *Phys. Rev. B: Condens. Matter Mater. Phys.* **1994**, *50*, 17953−17979.
(54) Kresse, G.; Joubert, D. *Phys. Rev. B: Condens. Matter Mater. Phys.* **1999**, *59*, 1758−1775.
(55) Vanpoucke, D. E. P.; Bultinck, P.; Van Driessche, I. *J. Comput. Chem.* **2013**, *34*, 405−417.
(56) Vanpoucke, D. E. P.; Van Driessche, I.; Bultinck, P. *J. Comput. Chem.* **2013**, *34*, 422−427.
(57) Vanpoucke, D. E. P. *Version 3.x* 2015, http://dannyvanpoucke.be.
(58) Lebedev, V. I.; Laikov, D. N. *Dokl. Akad. Nauk* **1999**, *366*, 741−745.
(59) Becke, A. D. *J. Chem. Phys.* **1988**, *88*, 2547−2553.
(60) Vanpoucke, D. E. P.; Olah, J.; De Proft, F.; Van Speybroeck, V.; Roos, G. *J. Chem. Inf. Model.* **2015**, *55*, 564−571.
(61) Shannon, R. D. *Acta Crystallogr., Sect. A: Cryst. Phys., Diffr., Theor. Gen. Crystallogr.* **1976**, *32*, 751.
(62) Basavaraju, N.; Priolkar, K. R.; Gourier, D.; Bessière, A.; Viana, B. *Phys. Chem. Chem. Phys.* **2015**, *17*, 10993−11000.
(63) Grebe, G.; Schulz, H. J. *Z. Naturforsch., A: Phys. Sci.* **1974**, *A29*, 1803−1819.
(64) Lehr, M. U.; Litzenburger, B.; Kreissl, J.; Pohl, U. W.; Selber, H. R.; Schulz, H. J.; Klimakow, A.; Worschech, L. *J. Phys.: Condens. Matter* **1997**, *9*, 753−763.
(65) Vivet, N.; Morales, M.; Levalois, M.; Doualan, J. L. *Opt. Lett.* **2010**, *35*, 983−985.
(66) Peppers, J.; Fedorov, V. V.; Mirov, S. B. *Opt. Express* **2015**, *23*, 4406−4414.

DOI: 10.1021/acs.inorgchem.5b02805
Inorg. Chem. 2016, 55, 2402−2412